Biosensors and Bioelectronics 72 (2015) 288–293

Contents lists available at ScienceDirect

Biosensors and Bioelectronics

journal homepage: www.elsevier.com/locate/bios

Fabrication of PMMA nanofluidic electrochemical chips with integrated microelectrodes

Junshan Liu [a,*], Liang Wang [a], Wei Ouyang [b,1], Wei Wang [b,c,**], Jun Qin [a], Zheng Xu [a], Shenbo Xu [a], Dan Ge [d], Longchang Wang [a], Chong Liu [a], Liding Wang [a]

[a] Key Laboratory for Micro/Nano Technology and System of Liaoning Province, Dalian University of Technology, Dalian, Liaoning 116024, China
[b] Institute of Microelectronics, Peking University, Beijing 100871, China
[c] National Key Laboratory of Science and Technology on Micro/Nano Fabrication, Peking University, Beijing 100871, China
[d] Chemical Engineering School, Dalian University of Technology, Dalian 116024, China

ARTICLE INFO

Article history:
Received 8 March 2015
Received in revised form
10 May 2015
Accepted 11 May 2015
Available online 12 May 2015

Keywords:
Nanofluidic
Microelectrode
PMMA
Electrochemical detection
Biosensor

ABSTRACT

A novel method based on plasma etching was proposed for monolithically integrating planar nanochannels and microelectrodes on a poly (methyl methacrylate) (PMMA) plate, and complete PMMA nanofluidic electrochemical chips with integrated microelectrodes were constructed by bonding with another PMMA plate containing microchannels. The fabrication sequences of nanochannels and microelectrodes were optimized. The oxygen plasma etching rate of PMMA nanochannels was studied, and the average rate was 15 nm/min under optimal conditions. An UV-ozone assisted thermal bonding method was developed to realize a low-temperature chip bonding, and the variations in width and depth of nanochannels before and after bonding were 2% and 5%, respectively. As a demonstration, a nanoparticle crystal (NPC)-based nanofluidic biosensor with integrated Ag microelectrodes was designed and fabricated. Sub-microchannel arrays with a depth of 400 nm and a width of 30 μm on the biosensor functioned as filters, and trapped 540 nm silica nanoparticles modified with streptavidin inside the connected microchannel to assemble the NPC. The interspaces in the NPC formed a three-dimensional nanochannel network with an equivalent diameter of 81 nm. By measuring the conductance across the NPC, a high quality nanofluidic sensing of biotin was achieved. The limit of detection was 1 aM, and the detection range was from 1 aM to 0.1 nM.

1. Introduction

Nanofluidics has attracted extensive interests over the last decade, and has been used in many applications, such as sample preconcentration (Chen et al., 2012), single molecule analysis (Park et al., 2010), biosensing (Regonda et al., 2013), enzymatic reaction kinetics (Wang et al., 2013), and ionic transport regulation (Zeng et al., 2014). Benefitting from its high sensitivity, label-free detection and ease of miniaturization and integration, electrochemical detection has been becoming one of the most popular detection methods for microchip analyses, and has been integrated with nanofluidic chips (Karnik et al., 2005; Martins et al., 2013a; Mela et al., 2004; Stein et al., 2004; Wolfrum et al., 2008). Initially, external electrodes, such as Ag or Pt wires, were inserted into the reservoir of the chip for electrochemical detection (Karnik et al., 2005; Mela et al., 2004; Stein et al., 2004). Recently, to improve the integration of chips or fulfill some special functions (e.g., redox cycling), microelectrodes have been integrated on the chip (Martins et al., 2013a; Regonda et al., 2013; Wolfrum et al., 2008).

While glass and silicon are still popular substrate materials for nanofluidic chips (Karnik et al., 2005; Mela et al., 2004; Park et al., 2010; Regonda et al., 2013; Stein et al., 2004; Wolfrum et al., 2008), polymers are getting increasing attention due to their low cost, biocompatibility and suitability for making disposable chips (Wang et al., 2013; Zeng et al., 2014). Several methods have been reported for fabricating polymer nanochannels, such as sacrificial etching (Eijkel et al., 2004), proton beam writing (Shao et al., 2006), focused-ion beam milling (Cannon et al., 2004) and a variety of replication techniques (Liu et al., 2013; Studer et al., 2002; Zhang et al., 2008). Meanwhile, a few methods have been explored to fabricate microelectrodes on polymer substrates, including electrode microchannel method (Rossier et al., 1999),

* Corresponding author at: Key Laboratory for Micro/Nano Technology and System of Liaoning Province, Dalian University of Technology, Dalian, Liaoning 116024, China. Fax: +86 411 8470 7940.
** Corresponding author. Fax: +86 411 8470 7940.
E-mail addresses: liujs@dlut.edu.cn (J. Liu), w.wang@pku.edu.cn (W. Wang).
[1] Present address: Department of Electrical Engineering and Computer Science, Massachusetts Institute of Technology, Cambridge, MA 02139, USA.

http://dx.doi.org/10.1016/j.bios.2015.05.031
0956-5663/

shadow mask method (Chen et al., 2001), screen printing (Kadara et al., 2009), electroless plating (McCarley et al., 2005), and photolithography techniques (Illa et al., 2010; Liu et al., 2011).

However, to our knowledge, there were no reports about fabricating polymer nanofluidic electrochemical chips with integrated microelectrodes. In order to facilitate the fluid supply, the nanochannel is typically integrated with a microchannel on either side. Therefore, a nanofluidic electrochemical chip mainly consists of microchannels, nanochannels and microelectrodes. In most cases, to avoid the troublesome alignment during the chip bonding process, nanochannels and microelectrodes were fabricated on the same plate (Martins et al., 2013a, 2013b; Wolfrum et al., 2008), while microchannels were made on another plate. However, unfortunately, most polymer nanochannel fabrication methods are not compatible with the microelectrode fabrication methods. Hence, it is very challenging to fabricate nanochannels and microelectrodes on the same polymer substrate and make an all-in-one chip. To solve this problem, Conde's group fabricated nanochannels and microelectrodes on a glass plate, and bonded this glass plate with a polydimethylsiloxane (PDMS) plate to make a glass/PDMS hybrid chip (Martins et al., 2013a, 2013b). Xia's group used external electrodes for PDMS/ polycarbonate or PDMS/glass hybrid chips (Wang et al., 2010; Wang et al., 2013).

Photolithography is most widely used to fabricate microelectrodes due to the perfect control of shape and dimensions (Illa et al., 2010; Liu et al., 2011; Martins et al., 2013b). Plasma etching is compatible with photolithography techniques, and has been proved to be a good method for fabricating polymer microstructures, such as waveguides (Inoue et al., 2003), microchannels (Rossier et al., 2002), and even nanochannels (Liu et al., 2012). In this study, a novel method based on plasma etching was proposed for monolithically integrating planar nanochannels and microelectrodes on a single poly (methyl methacrylate) (PMMA) plate, and complete PMMA nanofluidic electrochemical chips with integrated microelectrodes were for the first time constructed by bonding with another PMMA plate containing microchannels.

The surface modification of nanochannels is another challenge, especially for the application of biosensing (Mawatari et al., 2014; Shirai et al., 2014). Combining nanofluidic chips with the nanoparticle crystal (NPC) could be one of the effective approaches to the nanofluidic biosensing beacause the surface chemical properties of nanoparticles can be easily tuned. In our previous works, with a glass or silicon chip, the sensing principle, selectivity and specificity of the NPC-based nanofluidic biosensing have been demonstrated (Ouyang et al., 2013; Sang et al., 2013). However, it was found that there were several possible issues for ultra-high sensitive nanofluidic sensing by using silicon or glass as the chip substrate, such as a large background noise, non-transparent substrate (Si), a relatively long and expensive process, etc. On the contrary, PMMA has a lower bulk conductivity, which will facilitate to achieve a better signal-to-noise ratio and a higher sensitivity. Moreover, PMMA is good transparent and easy of fabrication.

Hence, in this work, to demonstrate the fabrication methods for nanofluidic electrochemical chips, a NPC-based PMMA nanofluidic biosensor with integrated Ag microelectrodes for biotin sensing was fabricated and tested.

2. Experimental methods

2.1. Design of the nanofluidic biosensor

The NPC-based nanofluidic biosensor shown in Fig. 1 is composed of a nanochannel plate (30 × 25 × 2 mm) with three sub-microchannel arrays and four Ag microelectrodes, and a microchannel plate (20 × 25 × 2 mm) with four microchannels and four reservoirs. Each sub-microchannel array includes two sub-microchannels and connects two adjacent microchannels. The sub-microchannel arrays work as filters, and sieve nanoparticles from the central microchannel for assembling the NPC. The depth of the sub-microchannel is 400 nm, which is smaller than the diameter of the silica nanoparticle used here (540 nm) to realize nanoparticle filtration. All sub-microchannels are 30 μm wide and 80 μm long. The interspaces in the NPC are at nano-scale, and connected with each other to form a three-dimensional nanochannel network. The equivalent diameter of the interspaces is 0.15 times the diameter of the nanoparticle (Zeng and Harrison, 2007), and equals 81 nm here. All microchannels are 150 μm wide, 7 μm deep and 3.5 mm long. Two 200 μm wide Ag microelectrodes across lateral microchannels are used for measuring the conductance across the NPC. The diameter of the reservoir is 2 mm.

2.2. Fabrication of nanofluidic electrochemical chips

The fabrication of nanofluidic electrochemical chips includes monolithic integration of planar nanochannels and microelectrodes, microchannel fabricating and chip bonding.

2.2.1. Monolithic integration of planar nanochannels and microelectrodes

Planar nanochannels and Ag microelectrodes were monolithically integrated on a PMMA plate by a method based on plasma etching, which is schematically depicted in Fig. 2: (a) A titanium layer (20 nm) and a silver layer (200 nm) were sputtered

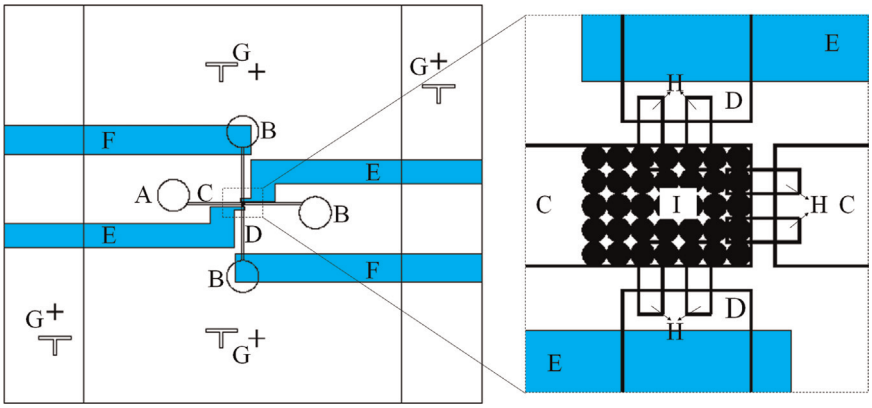

Fig. 1. Layout of the NPC-based nanofluidic biosensor. (A) sample reservoir, (B) waste reservoir, (C) central microchannel, (D) lateral microchannel, (E) detection electrode, (F) electrodes not used, (G) alignment mark, (H) nanochannel, and (I) nanoparticle.

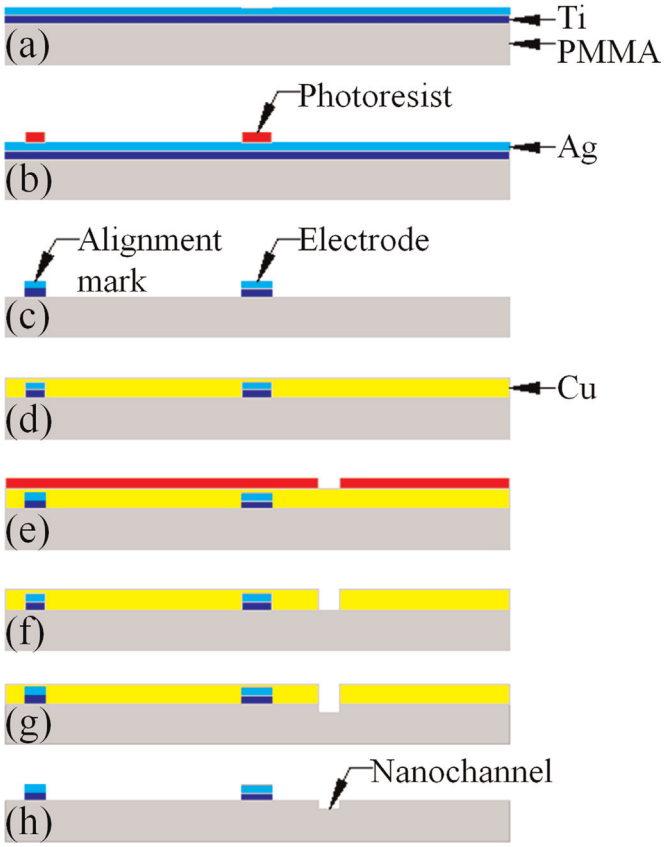

Fig. 2. Monolithic integration of planar nanochannels and Ag microelectrodes on a PMMA plate. (a) Sputtering of Ti and Ag layers; (b) photolithography; (c) etching Ag and Ti; (d) sputtering of Cu layer; (e) photolithography; (f) etching Cu; (g) oxygen plasma etching of PMMA; and (h) removing of Cu etching mask.

on a PMMA plate at a sputtering power of 300 W. (b) A positive photoresist (BP212, Kempur Microelectronics. Inc., China) was spin-coated on the silver layer at 2600 rpm for 30 s. The photoresist was exposed to UV light at a dose of 4.2 mJ/cm^2 for 30 s, and developed in 0.5% NaOH solution. While the recommended soft-baked and hard-baked temperatures of the photoresist is over 90 °C according to the manufacturer's instructions, the photoresist was baked at a lower temperature of 60 °C for a longer time of 1 h to avoid the thermal deformation of the PMMA plate. (c) The silver and titanium were etched in the mixture of NH_4OH and H_2O_2 (5:2, v/v) and buffered hydrofluoric acid, respectively. The residual photoresist was exposed to UV light for 3 min and removed by 0.5% NaOH solution. (d) A copper layer (100 nm) was sputtered on the PMMA plate. (e) The positive photoresist was patterned on the copper layer. (f) The copper was etched in 2.5% HNO_3 solution to form an etching mask, and the photoresist was also removed by 0.5% NaOH solution. (g) The PMMA plate was placed in a plasma cleaner (DQ-500, China Electronics Technology Group Corporation, China), and the exposed PMMA was etched by oxygen plasma to form the nanochannel. (h) The copper etching mask was removed by 2.5% HNO_3 solution.

2.2.2. Microchannel fabricating

The microchannel was fabricated by a hot embossing method (Liu et al., 2006). In brief, a silicon mold was made based on photolithography and anisotropic wet etching. A PMMA plate was placed on the silicon mould, and embossed at a temperature of 110 °C and a pressure of 1.4 MPa for 5 min by using a homemade embossing machine. The control accuracies of the temperature and pressure of this machine are 0.2 °C and 20 N, respectively. The microchannel plate was demoulded from the silicon mold at 65 °C. Four access holes as reservoirs were drilled.

2.2.3. Chip bonding

The chip was bonded by an UV-ozone assisted thermal bonding method. Both the nanochannel plate and the microchannel plate were placed in an UV-ozone cleaning chamber (BZD250-S, HWOTECH Co. Ltd., China) for the surface treatment. The low pressure mercury vapor grid lamp emits UV lights at 185 nm and 254 nm wavelengths. The output power of the lamp was about 10 mW/cm^2 according to the manufacturer's specification. The lamp was warmed for 15 min. The plates were treated at a distance of 7.5 cm from the lamp for 5 min. After the treatment, these two plates were aligned with the help of a home-made aligning device (Xu et al., 2009), and then bonded together at a temperature of 70 °C and a pressure of 1.0 MPa for 20 min.

2.3. Testing of the nanofluidic biosensor

Monodisperse streptavidin-coated silica nanoparticle suspension was purchased from Bangs Laboratories Inc. (Category Code: CS01N). The diameter of the nanoparticle was 540 nm. The concentration of the nanoparticle suspension was 10 mg/ml, and diluted to 200 μg/ml in deionized (DI) water for the experiment. D-biotin (Product Number: B4501) from Sigma-Aldrich was used as the target molecule. D-biotin solutions with concentrations ranging from 10^{-18} M to 10^{-5} M were prepared in DI water.

Streptavidin-coated nanoparticle suspension was introduced into the central microchannel from the reservoir A at a flow rate of 5 nl/s by a syringe pump. The NPC was formed at the end of the central microchannel due to the confinements of three groups of sub-microchannels. Then, the biotin solution was also loaded into the central microchannel from the reservoir A at a flow rate of 5 nl/s. After 30 min continuous injection of the biotin solution, the ion conductance across the NPC was measured and extracted from the *I–V* curve by a sourcemeter (2611B, Keithley Instruments, Inc.). DC voltage from −1 V to +1 V with a step of 50 mV and a holding time of 60 s was applied for the *I–V* testing. The microchip was washed with DI water after every biotin injection and before measurement.

3. Results and discussion

3.1. Optimization of the fabrication sequence

While the processes for fabricating nanochannels and microelectrodes (Fig. 1) are completely compatible with each other, the fabrication sequence is of great importance to the feasibility of monolithic integration of nanochannels and microelectrodes. The oxygen plasma ething process generates heat, and the heat will increase the temperature of PMMA plates. The thermal expansion coefficient of PMMA ($\sim 80 \times 10^{-6}$/K) is much larger than that of metals, so tensile stress in metal microelectrodes would be induced from the thermal expansion coefficient mismatches if microelectrodes were first fabricated. Accordingly, some cracks in microelectrodes could be caused if the stress was large enough. Considering this problem, initially nanochannels were first fabricated. Some alignment marks (cross-shaped or T-shaped channels with a micro-scale width and a same depth as nanochannels) were simultaneously fabricated with the nanochannel because a strict alignment between nanochannels and microelectrodes was required. However, since these channel marks were very shallow, it was very difficult to recognize them by the bottom objectives on the mask alignmer (MA/BA6, SUSS Micro Tec) when executing the subsequent exposure process for patterning microelectrodes.

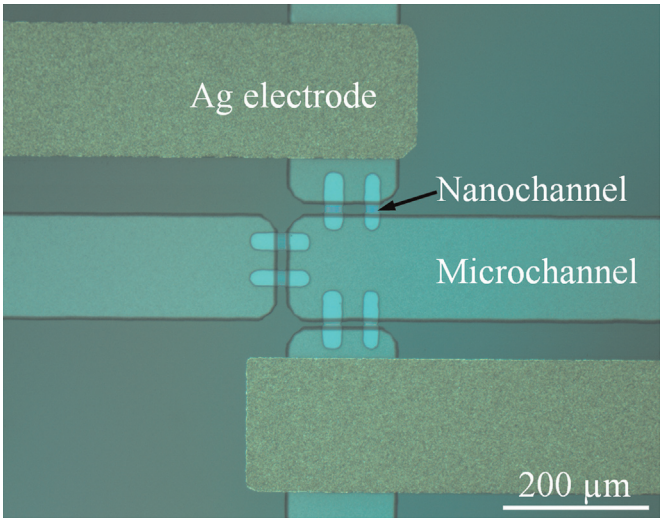

Fig. 3. The enlarged view of micro/sub-microchannels and Ag microelectrodes on the nanofluidic biosensor.

Hence, Ag microelectrodes and Ag alignment marks (Fig. 1) had to be first fabricated. It was easy to find the Ag marks when executing the exposure process for patterning nanochannels. In order to monitor the temperatue of PMMA plates and obviate large thermal stress in microelectrodes, the temperature of the PMMA plate was measured by a surface temperature indicating strip (TMC Hallcrest, UK) during the plasma etching process. It was observed that the highest temperature of the PMMA plate was lower than 37 °C after continuous etching for 5 min. Hence, the etching process can stop for a while if a longer etching time is required, and then restart again. For the 400 nm deep sub-microchannles on the nanofluidic biosensor, the etching process was divided into five periods. In each period, the etching time was 5 min, and the stopping time was also 5 min. That is, the whole etching time was 25 min, and no cracks in Ag microelectrodes were found (Fig. 3).

3.2. Oxygen plasma etching

Planar nanochannels were fabricated by a simple oxygen plasma ethcing process. The etching process was performed by using a commonly used plasma cleaner instead of some special and expensive tools, such as inductively coupled plasma (ICP) or reactive ion etching (RIE) systems, which makes it accessible by most academic institutions. The process parameters of the plasma cleaner were optimized based on previously published procedures (Liu et al., 2012). Under the optimized condition with RF power of 60 W and chamber pressure of 200 Pa, the dependence of the etching depth of a planar nanochannel with a width of 2 μm on etching time was studied. The depth of nanochannels was measured by a stylus profiler (ET4000M, Kosaka Laboratory Ltd., Japan). As shown in Fig. 4a, the depth of nanochannels presented a good linear relationship with the etching time, and the average etching rate was about 15 nm/min. Therefore, the depth of nanochannels can be precisely controlled, and thus the whole nanofluidic electrochemical chip is repeatable. Fig. 4b shows a planar nanochannel with a depth of 80 nm and a surface roughness (R_a) less than 2 nm.

3.3. UV-ozone assisted thermal bonding

The chip bonding temperature is often close to the glass transition temperature (T_g) of polymers, and nanochannels will deform during the bonding process. The T_g of PMMA is 105 °C. We once developed a plasma-assisted thermal bonding method to realize a low-temperature (85 °C) bonding of PMMA nanofluidic chips (Liu et al., 2009, 2012). However, under the same bonding condition, it was observed that sub-microchannels on the nanofluidic biosensor collapsed. This could be attributed to the fact that these sub-microchannels had a much larger aspect ratio of width to depth (75), which makes them more prone to be deformed. Thus, to further decrease the bonding temperatue, an UV-ozone assisted thermal bonding method was developed. It has been demonstrated that the decrease of the water contact angle implied a corresponding drop in T_g (Bhattacharyya and Klapperich, 2007). Therefore, the water contact angle on the surface of the treated PMMA plate was measured and used to optimize the UV-ozone exposure time. As shown in Fig. 5, the minimum water contact angle was 29.9° when the exposure time was 5 min, which is about 14° smaller than that obtained from plasma treatment (43.6°) (Liu et al., 2009). Hence, the nanochannel plate and the microchannel plate were exposed to UV-ozone for 5 min prior to bonding in all subsequent experiments. The bonding temperature was optimized when the bonding pressure and time were kept constant. The optimized temperature was 70 °C, which is 15 °C lower than that used in the plasma-assisted thermal bonding method (Liu et al., 2012). Five nanofluidic biosensors were consecutively bonded at 70 °C, and three out of five chips presented both complete bonding and unblocked channels. The width of the sub-microchannels was changed from 30.9 μm to 31.5 μm, and the depth from 433 nm to 411 nm after bonding. The variations in width and depth were 1.9% and 5.1%, respectively.

3.4. Characterization of the nanofluidic biosensor

It has been demonstrated that the surface charge dominated the ion conductance of the NPC at low bulk concentration

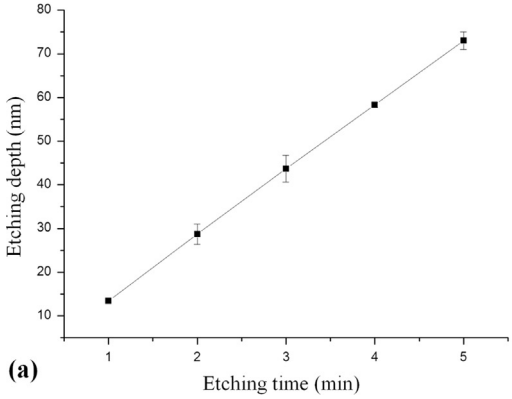

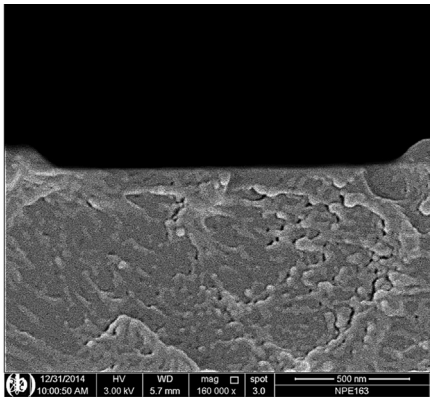

Fig. 4. (a) Etching depth of the nanochannel as a function of etching time; and (b) the cross section of a planar nanochannel with a width of 2 μm and a depth of 80 nm.

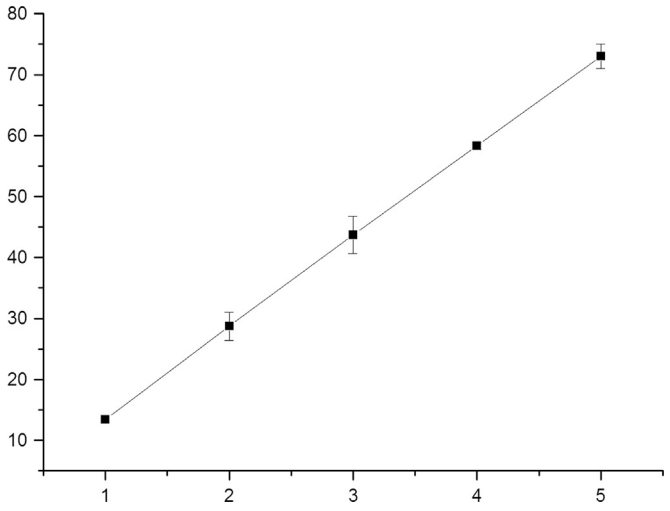

Fig. 5. Effect of the UV-ozone exposure time on the water contact angle on the PMMA surface.

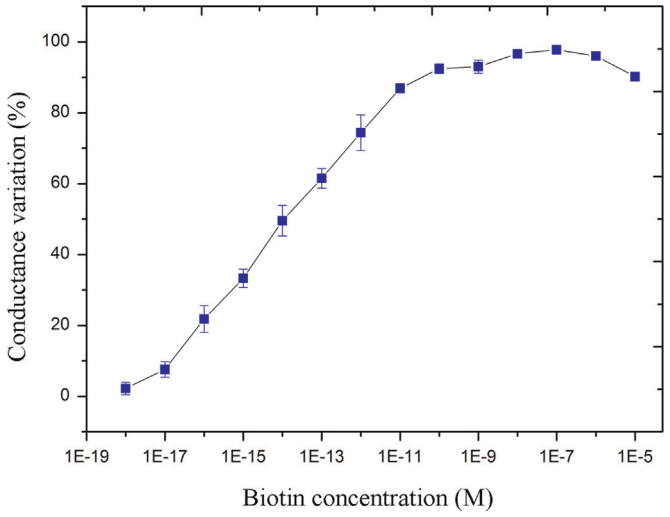

Fig. 6. Conductance variation varied with the biotin concentrations (log scale).

condition, the surface charge density would be changed due to the reaction between the immobilized probe molecule on the nanoparticle and the dissociated target molecule, and the induced conductance variation could be used for sensing the concentration of the target molecule (Lei et al., 2010; Sang et al., 2013).

Here streptavidin coated on the nanoparticle was the probe molecule and negatively charged, and biotin was the target molecule and positively charged. The conductance variation (Δ) caused by the binding of biotin and streptavidin was shown in Fig. 6. The variation was calcualted as $(G_b - G_a)/G_b$ where G_b and G_a denoted conductances of the NPC before and after the biotin binding. Compared with the NPC formed in a micropore (Lei et al., 2010), the biosensor proposed here exhibited a much higher sensitivity. The limit of detection (LOD) for biotin was 1 aM, with a conductance variation of 2.3%, which is nine orders of magnitude lower than that obtained in the micropore scheme (Lei et al., 2010). The conductance variation was up to 93.8% when the biotin concentration was 1 nM, while the value in the micropore scheme was only 11.8% when the biotin concentration was 5 nM (Lei et al., 2010). The huge improvement in the sensitivity mainly attributed to the following three factors. First of all, the continous injection of the biotin solution here increased the binding opportunity of biotin and streptavidin. The continous sample loading kept the biotin concentration constant and shifted the chemical equilibrium towards the binding. Moreover, differing from the diffusion in the micropore, the flow of the biotin molecule caused by the continuous injection increased the collision frequency of biotin to the nanoparticle, which in turn increased the binding opportunity. Second, the integrated detection electrode here was very close to the NPC, with a distance of only 80 μm, which is impossible for the external Pt wire used in the micropore scheme (Lei et al., 2010), and the small distance contributes to improve the sensitivity (Martins et al., 2013a). Third, for the micropore scheme, due to the low controllability of the self-assembly of nanoparticles, some of the nanoparticles would inevitably be outside the micropore. Streptavidin on these nanoparticles also consumed biotin, but had little contributions to the ion conductance. Accordingly, the detection sensitivity would be lowered.

As shown in Fig. 6, at the beginning, the conductance variation increased with the biotin concentration, and the variation was up to 93.2% when the concentration was 0.1 nM. Then the binding of biotin and streptavidin reached saturation, and there was no significant increase in the variation with the the increase of biotin concentraiton. Moreover, the variation began to decrease at the concentration of 0.1 μM. It is believed that further increasing the concentration of biotin made excessive biotin be physically adsorbed on the nanoparticle surface, which turned the surface positively charged and reduced the conductance variation (Lei et al., 2010). Therefore, the nanofluidic biosensor can provide a wide detection range of 1 aM to 0.1 nM for biotin. Within this detection range, the concentration of biotin is far less than the intrinsic H^+ (the main carrier inside the nanoparticle crystal) concentration of water, i.e. around 0.1 μM. Therefore, the target molecule, biotin here, will not contribute to the conductivity changes directly as a carrier. The measured signal came from the surface charge density variation, i.e. the biotin binding to the streptavidin modified on the nanoparticles.

4. Conclusions

PMMA nanofluidic electrochemical chips with integrated microelectrodes were presented in this study. To fabricate this complete PMMA chip, a novel method based on plasma etching was proposed for monolithic integration of planar nanochannels and microelectrodes on a single PMMA plate, and an UV-ozone assisted thermal bonding method was developed for assembling the chip at a low temperature. The fabrication of the nanofluidic electrochemical chip is compatible with well-developed microfabrication techniques. Hence, the shape and dimensions of micro/nanochannels and microelectrodes on the chip can be precisely controlled, and the chip can be mass produced at low cost. By combining nanofluidic chips with the NPC, a nanofluidic biosensor was demonstrated. The biosensor exhibits an excellent sensitivity and a wide detection range, and holds great potential for a variety of biosensing applications.

Acknowledgments

This work was supported by the National Natural Science Foundation of China (51475080, 51321004, 31300809, 91323304), the National High-tech R&D Program of China (2012AA040406), the Fundamental Research Funds for the Central Universities (DUT14QY21), the 985-III program (clinical applications) in Peking University and the Open Fund of the State Key Laboratory of Precision Measuring Technology and Instruments (Tianjin University).

References

Bhattacharyya, A., Klapperich, C.M., 2007. Lab Chip 7 (7), 876–882.
Cannon, D.M., Flachsbart, B.R., Shannon, M.A., Sweedler, J.V., Bohn, P.W., 2004. Appl. Phys. Lett. 85 (7), 1241–1243.
Chen, D.C., Hsu, F.L., Zhan, D.Z., Chen, C.H., 2001. Anal. Chem. 73 (4), 758–762.
Chen, W., Jin, B., Hu, Y., Lu, Y., Xia, X., 2012. Small 8 (7), 1001–1005.
Eijkel, J.C.T., Bomer, J., Tas, N.R., van den Berg, A., 2004. Lab Chip 4 (3), 161–163.
Illa, X., Ordeig, O., Snakenborg, D., Rodríguez, A.R., Compton, R.G., Kutter, J.P., 2010. Lab Chip 10 (10), 1254–1261.
Inoue, S.I., Kajikawa, K., Aoyagi, Y., 2003. Appl. Phys. Lett. 82 (18), 2966–2968.
Kadara, R.O., Jenkinson, N., Banks, C.E., 2009. Electrochem. Commun. 11 (7), 1377–1380.
Karnik, R., Castelino, K., Fan, R., Yang, P., Majumdar, A., 2005. Nano Lett. 5 (9), 1638–1642.
Liu, J., Jin, X., Sun, T., Xu, Z., Liu, C., Wang, J., Chen, L., Wang, L., 2013. Microsyst. Technol. 19 (4), 629–634.
Liu, J., Liu, C., Guo, J.H., Wang, L.D., 2006. J. Mater. Process. Technol. 178 (1–3), 278–282.
Liu, J., Qiao, H., Liu, C., Xu, Z., Li, Y., Wang, L., 2009. Sens. Actuators B – Chem. 141 (2), 646–651.
Liu, J., Qiao, H., Xu, Z., Liu, C., Wang, J., Du, L., Zhang, X., Wang, L., 2012. Micro Nano Lett. 7 (2), 159–162.
Liu, J., Wang, J., Chen, Z., Yu, Y., Yang, X., Zhang, X., Xu, Z., Liu, C., 2011. Lab Chip 11 (5), 969–973.
Lei, Y., Xie, F., Wang, W., Wu, W., Li, Z., 2010. Lab Chip 10 (18), 2338–2340.
Martins, D.C., Chu, V., Conde, J.P., 2013a. Biomicrofluidics 7 (3), 034111.
Martins, D.C., Chu, V., Conde, J.P., 2013b. Appl. Phys. Lett. 103 (25), 253112.
Mawatari, K., Kazoe, Y., Shimizu, H., Pihosh, Y., Kitamori, T., 2014. Anal. Chem. 86 (9), 4068–4077.
McCarley, R.L., Vaidya, B., Wei, S., Smith, A.F., Patel, A.B., Feng, J., Murphy, M.C., Soper, S.A., 2005. J. Am. Chem. Soc. 127 (3), 842–843.
Mela, P., Tas, N.R., Berenschot, E.J.W., van Nieuwkasteele, J., van den Berg, A., 2004. Electrophoresis 25 (21–22), 3687–3693.
Ouyang, W., Sang, J., Shi, Y., Wang, W., Chu, M., Wang, Y., Li, H., Zhang, H., Wu, W., Li, Z., 2013. Proceeding of the 17th International Conference on Miniaturized Systems for Chemistry and Life Sciences, pp. 663–665.
Park, S., Huh, Y.S., Szeto, K., Joe, D.J., Kameoka, J., Coates, G.W., Edel, J.B., Erickson, D., Craighead, H.G., 2010. Small 6 (21), 2420–2426.
Regonda, S., Tian, R., Gao, J., Greene, S., Ding, J., Hu, W., 2013. Biosens. Bioelectron. 45, 245–251.
Rossier, J.S., Roberts, M.A., Ferrigno, R., Girault, H.H., 1999. Anal. Chem. 71 (19), 4294–4299.
Rossier, J.S., Vollet, C., Carnal, A., Lagger, G., Gobry, V., Girault, H.H., Michel, P., Reymond, F., 2002. Lab Chip 2 (3), 145–150.
Sang, J., Du, H., Wang, W., Chu, M., Wang, Y., Li, H., Zhang, H., Wu, W., Li, Z., 2013. Biomicrofluidics 7 (2), 024112.
Shao, P., van Kan, A., Wang, L., Ansari, K., Bettiol, A.A., Watt, F., 2006. Appl. Phys. Lett. 88 (9), 093515.
Shirai, K., Mawatari, K., Kitamori, T., 2014. Small 10 (8), 1514–1522.
Stein, D., Kruithof, M., Dekker, C., 2004. Phys. Rev. Lett. 93 (3), 035901.
Studer, V., Pepin, A., Chen, Y., 2002. Appl. Phys. Lett. 80 (19), 3614–3616.
Wang, C., Li, S., Wu, Z., Xu, J., Chen, H., Xia, X., 2010. Lab Chip 10 (5), 639–646.
Wang, C., Ye, D., Wang, Y., Lu, T., Xia, X., 2013. Lab Chip 13 (8), 1546–1553.
Wolfrum, B., Zevenbergen, M., Lemay, S., 2008. Anal. Chem. 80 (4), 972–977.
Xu, Z., Wen, J., Liu, C., Liu, J., Du, L., Wang, L., 2009. Microfluid. Nanofluid. 7 (3), 423–429.
Zeng, L., Yang, Z., Zhang, H., Hou, X., Tian, Y., Yang, F., Zhou, J., Li, L., Jiang, L., 2014. Small 10 (4), 793–801.
Zeng, Y., Harrison, D.J., 2007. Anal. Chem. 79 (6), 2289–2295.
Zhang, L., Gu, F., Tong, L., Yin, X., 2008. Microfluid. Nanofluid. 5 (6), 727–732.